

Three-dimensional morphometry of the human thoracic aorta using centerline analysis based on least-squares plane fitting



Hiroshi Nagamine, MD, Kenji Kishita, MD, Yuta Tsukada, MD, Hiroshi Nagano, MD, and Mitsuru Asano, MD

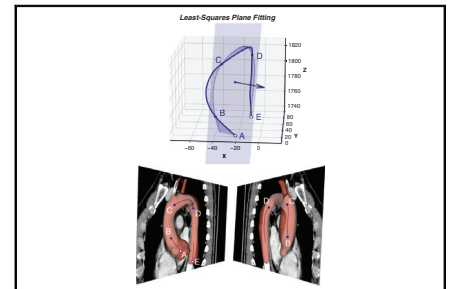
ABSTRACT

Objective: A novel approach to 3-dimensional morphometry of the thoracic aorta was developed by applying centerline analysis based on least-squares plane fitting, and a preliminary study was conducted using computed tomography imaging data.

Methods: We retrospectively compared 3 groups of patients (16 controls without aortic disease, and 16 cases each with acute type B aortic dissection and congenital bicuspid aortic valve). In addition to the standard assessment indices for curvature κ and torsion τ , we conducted coordinate transformation based on the least-squares plane, divided the centerline into 3 representative features (transverse, anterior-posterior, and longitudinal displacements), and analyzed the overall and local displacement in each direction. The transverse displacement, represented by the distance of the centerline from the least-squares plane, was curve-fitted to the damped oscillation waveform. Thereafter, damped oscillation parameters were compared for each group.

Results: Curvature κ exhibited a bimodal distribution, with peaks observed in the ascending aorta and aortic arch, and torsion τ exhibited a transition from positive to negative values in the arch. There were significant differences in the mean displacement between the groups for each direction (transverse $P = .0083$, anteroposterior $P = .010$, longitudinal $P = 1.32 \times 10^{-6}$). Furthermore, interval integral analysis revealed that several intervals exhibited significant differences between groups in each direction. The amplitude of damped oscillation parameters was significantly larger in the bicuspid aortic valve group than in the control and type B aortic dissection groups.

Conclusions: The novel analytical approach permitted a quantitative assessment of the 3-dimensional morphological differences between the control, type B aortic dissection, and bicuspid aortic valve groups. (JTCVS Open 2024;22:144-55)



Least-squares plane fitting to centerline of thoracic aorta.

CENTRAL MESSAGE

A novel approach to 3-dimensional morphometry of the thoracic aorta was developed by applying centerline analysis based on least-squares plane fitting, and a preliminary study was conducted.

PERSPECTIVE

This study presents a novel analytical approach based on the optimal plane for the centerline analysis of the thoracic aorta. This novel approach provides a more comprehensive, versatile, and standardized methodology for geometrically visualizing the shape and characteristics of 3-dimensional curves that are challenging to accurately capture in their entirety using conventional techniques.

From the Department of Cardiovascular Surgery, Seirei Mikatahara General Hospital, Hamamatsu, Japan.

Institutional Review Board Approval: This study was approved by our local ethics committee (No. 23-75; March 7, 2024). Written informed consent was not necessary because of the retrospective observational nature of the study.

Received for publication June 30, 2024; revisions received Aug 17, 2024; accepted for publication Sept 18, 2024; available ahead of print Oct 21, 2024.

Address for reprints: Hiroshi Nagamine, MD, Department of Cardiovascular Surgery, Seirei Mikatahara General Hospital, 3453 Mikatahara-cho, Chuo Ward, Hamamatsu, Shizuoka 433-8558, Japan (E-mail: h.nagamine@me.com).


2666-2736

Copyright © 2024 The Author(s). Published by Elsevier Inc. on behalf of The American Association for Thoracic Surgery. This is an open access article under the CC BY-NC-ND license (<http://creativecommons.org/licenses/by-nc-nd/4.0/>).

<https://doi.org/10.1016/j.xjon.2024.09.016>

Abbreviations and Acronyms

3D	= 3-dimensional
AoR	= aortic root
Arch	= aortic arch
AscAo	= ascending aorta
BAV	= bicuspid aortic valve
CT	= computed tomography
DesAo	= descending aorta
ECG	= electrocardiogram
LCCA	= left common carotid artery
TBAD	= type B aortic dissection

 Video clip is available online.

The thoracic aorta, which consists of the aortic root (AoR), ascending aorta (AscAo), aortic arch (Arch), and descending aorta (DesAo), has a characteristic 3-dimensional (3D) morphology with significant tortuosity, in addition to its large curvature inverting more than 180° from the cranial to caudal direction.¹ Due to its tortuosity, the thoracic aorta does not lie in a single plane and is therefore distorted in three dimensions, making it difficult to grasp its complex spatial geometry.²

The 3D geometry of the thoracic aorta, including its curvature and tortuosity, has been shown to play a significant role in the development of aortic aneurysms and acute aortic dissections.^{3,4} Recent studies using hydrodynamic simulations have shown that the strong bending and 3D twisting of the aorta cause perturbations in the blood flow pattern that affects the vessel wall and lead to the formation of atherosclerotic lesions, dissections, and aortic aneurysms.⁵⁻⁷

Blood flow patterns in the thoracic aorta depend on its 3D luminal structure, which is determined by the vessel diameter and vessel centerline. The centerline of the thoracic aorta, represented as a 3D spatial curve, is tightly defined by its differential-geometric properties, specifically curvature κ and torsion τ . These properties are mathematically quantified using Frenet-Serret formulas and are fundamental to understanding the spatial behavior of the curve.^{8,9} To date, only a few reports have examined the 3D morphology of the thoracic aorta in terms of centerline curvature κ and torsion τ , and their relationship to disease.¹⁰⁻¹²

In addition to the standard assessment indices for curvature κ and torsion τ , we present a new type of centerline analysis that incorporates the least-squares plane: an optimal plane (Figure 1). This novel approach provides a more comprehensive, versatile, and standardized methodology for geometrically visualizing the shape and characteristics of 3D curves that are challenging to accurately capture in their entirety using conventional techniques.

This report presents a centerline analysis of the thoracic aorta in 16 controls without aortic disease, 16 cases of acute type B aortic dissection (TBAD), and 16 cases of congenital bicuspid aortic valve (BAV). This analysis was conducted preliminarily using new indices based on the optimal plane. Furthermore, the vertical distance of the centerline from the optimal plane, which exhibits a damped oscillation pattern, was analyzed by fitting a damped oscillation waveform. These novel approaches provide a new perspective on characteristics of the 3D morphology of the thoracic aorta.

MATERIALS AND METHODS**Study Groups and Clinical Data**

We retrospectively compared 3 groups of patients (16 controls without aortic disease, 16 cases with TBAD, and 16 cases with BAV). The control group without aortic disease ($n = 16$) consisted of patients who underwent surgical treatment for mitral regurgitation or atrial septal defect in our hospital between September 2013 and November 2023 and underwent preoperative contrast-enhanced computed tomography (CT) imaging. The TBAD group ($n = 16$) consisted of patients who were treated for acute TBAD in our hospital between June 2006 and April 2023 and who underwent contrast-enhanced CT within 24 hours after the onset of dissection, excluding those who were older than age 65 years and whose image accuracy did not meet the requirements for analysis. The BAV group ($n = 16$) consisted of patients who underwent surgical treatment for congenital BAV in our hospital between April 2014 and November 2023 and underwent preoperative contrast-enhanced CT scan of the thoracic aorta. In addition to CT image data, the following parameters were collected: date of birth, date of CT examination, height, weight, sex, and diagnosis of hypertension. This study was approved by our local ethics committee (No. 23-75; March 7, 2024). Written informed consent was not necessary because of the retrospective observational nature of the study.

Image Acquisition

In the control and BAV groups, CT angiography was performed using an 80-detector-row CT scanner (Aquilion Prime SP, Toshiba Medical Systems) before March 2021 and a 320-detector-row CT scanner (Aquilion One Nature Edition, Canon Medical Systems) after March 2021. Electrocardiogram (ECG)-synchronized imaging (0.5-mm slice thickness) was performed in 6 patients (37.5%) in the control group and 14 patients (87.5%) in the BAV group who required coronary artery evaluation, whereas non-ECG-synchronized imaging (1-mm slice thickness) was performed in the remaining cases. In the TBAD group, CT angiography (1.25-mm slice thickness) was performed in the emergency department using a 64-detector-row CT scanner (GE Revolution EVO CT Scanner, GE Medical Systems) without the time-consuming ECG-synchronized imaging.

Classification of Aortic Arch Types

According to the report by Marrocco-Trischitta and colleagues,¹³ aortic arch type was determined by the vertical distance from the origin of the brachiocephalic trunk to the top of the arch (type I: <1 diameter of the left common carotid artery [LCCA], type II: 1 to 2 diameters of the LCCA, or type III: >2 diameters of the LCCA). The aortic arch was classified on multiplanar reconstruction images using the 3D image analysis system Synapse Vincent (Fujifilm Medical Co).

Aorta Segmentation and Centerline Extraction

The open-source software 3D Slicer was used to segment the thoracic aorta from CT images and create a surface model with contour smoothing. In the TBAD group, the entire aorta, including both true and false lumens,

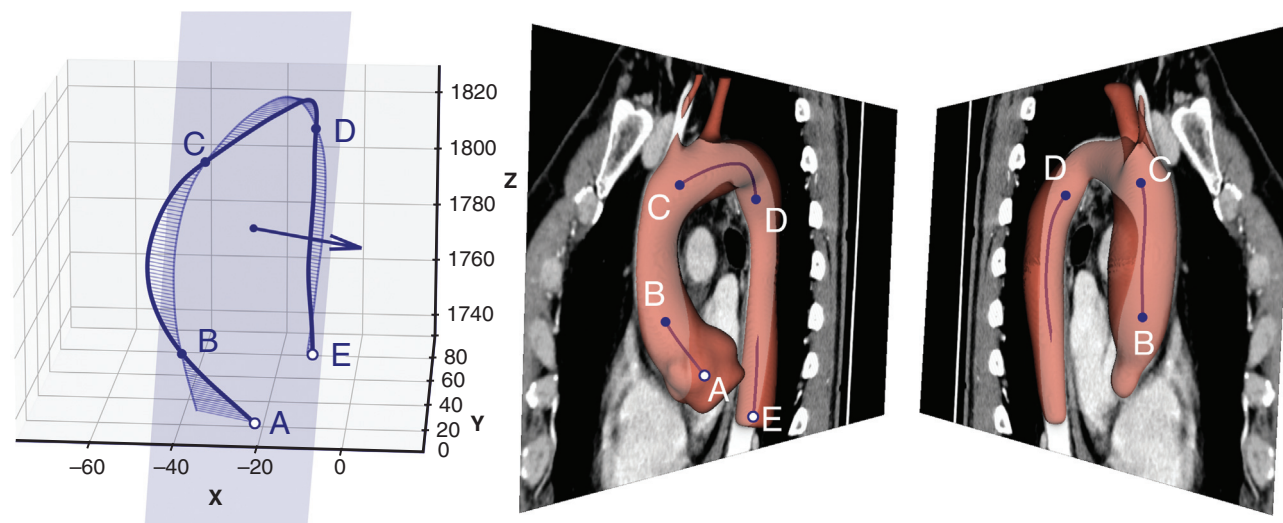


FIGURE 1. Least-squares plane fitting to centerline of thoracic aorta. *Left panel, bold blue line, centerline of thoracic aorta; light blue area, least-squares plane (optimal plane); thin light blue line, vertical distance from centerline to optimal plane; light blue line, projection line of centerline onto optimal plane. Middle and right panels, Three-dimensional surface model of the thoracic aorta, with a multiplanar reconstruction image of an optimized plane superimposed upon it. The starting point of the centerline is A○, the ending point is E○, and the intersection points of the centerline and the optimal plane are B●, C●, and D●, in that order.*

was segmented for centerline extraction. The centerline data set was generated from surface model using the Vascular Modeling Toolkit module in 3D Slicer. No Laplacian smoothing filter was used for centerline extraction.

Data Standardization: Data Scaling and Coordinate Transformation Based on Optimal Plane

To standardize individual centerline measurement data into a form that can be aligned to the same reference and compared, data scaling, and coordinate transformation based on the optimal plane were carried out in the following steps.

- Identification of the center of gravity of centerline point cloud data, extending from the aortic valve annulus to the descending aorta at the same level as the aortic valve annulus.
- Parallel shift of 3D coordinates with the center of gravity serving as the origin.
- Scaling such that the average distance of centerline point cloud data from the center of gravity is 100%.
- Derivation of the optimal plane (least-squares plane fitting): The unit normal vector of the least-squares plane was derived from singular value decomposition of the scaled centerline point cloud data. The plane containing the center of gravity was then identified as the least-squares plane. The normal vector of the least-squares plane for each group is illustrated in Figure E1.
- Rotational coordinate transformation with the optimal plane as the plane $x = 0$.

With data standardization, the x -coordinate is defined as the vertical distance between the optimum plane and the centerline, which represents the transverse displacement. In contrast, the sign-transformed y -coordinate represents the anterior-posterior displacement, whereas the z -coordinate is used to represent the longitudinal displacement (Figure 2, upper row).

3D Curve Fitting for Discrete Point Data of Centerlines

3D curve fitting was conducted using discrete point data of the centerline. Curve regression was performed using a fifth-order B-spline curve and

the regularized least-squares method.⁸ The number of control points was set to 20, and regularization terms were second- and third-order derivatives. The optimization parameter lambda to minimize mean square error was obtained through cross-validation using Optuna (version 3.5.0), an open source hyperparameter optimization framework (Preferred Networks, Inc).

Calculation of Curvature κ and Torsion τ Based on Frenet-Serre Formulas

The centerline's curvature κ and torsion τ were calculated at 200 equally spaced measurement points using Frenet-Serre formulas with NURBS-Python (*geomdl*) (version 5.3.1), an object-oriented B-Spline and Non-Uniform Rational B-Splines evaluation library. Curvature κ and torsion τ calculated from higher-order derivative values are subject to many data fluctuations, variations, and noise. Therefore, a moving average was applied to the data to smooth them out (smoothing window was set at 20 measurement points).

New Evaluation Indices Based on Optimal Plane

Following the implementation of data scaling, coordinate transformation, and curve fitting, the transverse displacement, represented by the x -coordinate, exhibited a damped oscillation pattern. The anterior-posterior displacement, represented by the sign-transformed y -coordinate, exhibited an inverse S-shaped curve pattern, whereas the longitudinal displacement, represented by the z -coordinate, exhibited an upward convex curve pattern (Figure 2).

These patterns, derived from 200 equally spaced 3D coordinates from the start to the end of the thoracic aortic centerline, were compared in each group as new evaluation metrics based on the optimal plane. Specifically, the mean value of displacement for each case was employed for overall comparison, and the integral value of the interval divided by the sign transformation point for each case (indicated as T1, T2, and T3 for transverse displacement; AP1 and AP2 for anteroposterior displacement; and L1, L2, and L3 for longitudinal displacement in the lower part of Figure 2) was employed for local comparison as evaluation indices.

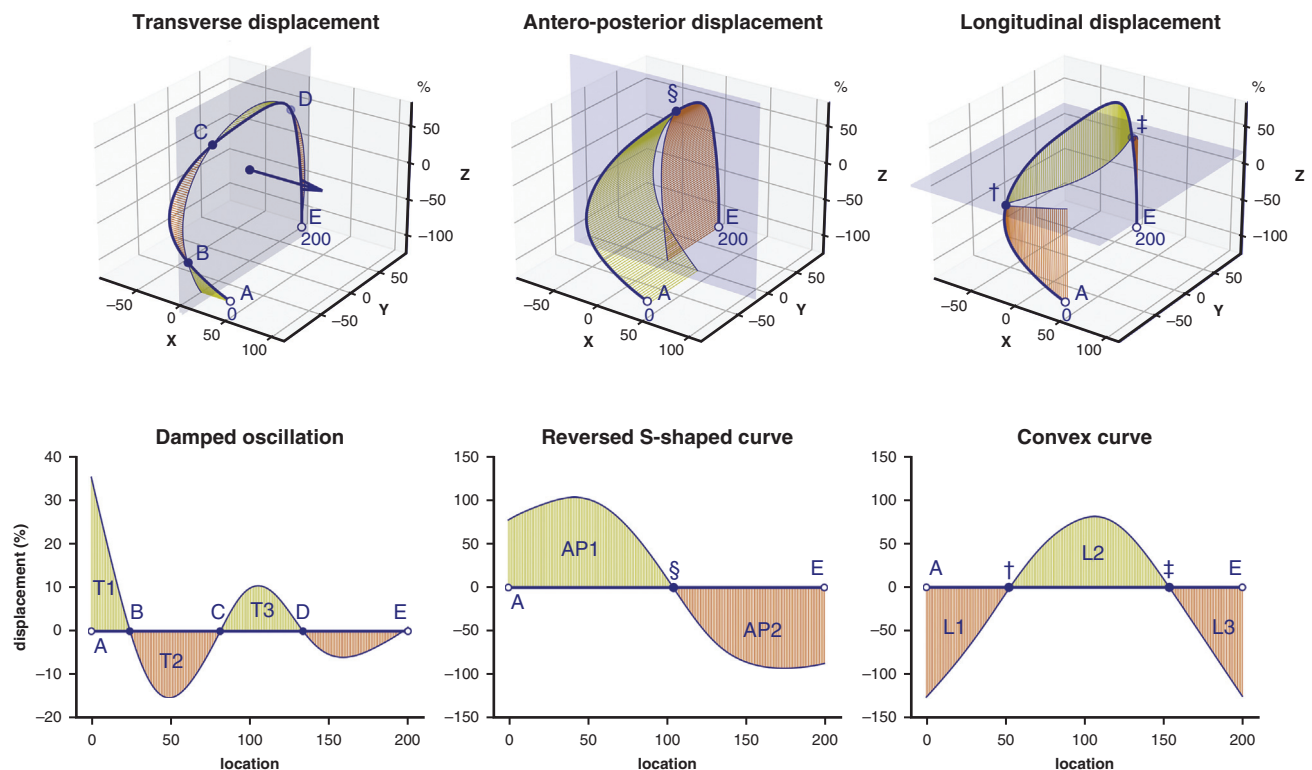


FIGURE 2. Coordinate transformation based on optimal plane. Coordinate transformation with an optimization plane yielded the following results: transverse displacement, represented by the x -coordinate, exhibited a damped oscillation pattern (*left column*); anterior-posterior displacement, represented by the sign-transformed y -coordinate, exhibited an inverse S -shaped curve pattern (*center column*); longitudinal displacement, represented by the z -coordinate, exhibited an upward convex curve pattern (*right column*). Regions (interval integrals: T1, T2, T3, AP1, AP2, L1, L2, L3) indicated in yellow and orange and classified according to the sign conversion points were employed as evaluation indices.

Analysis of Damped Oscillation Patterns for Transverse Displacement

The transverse displacement was fitted to the damped oscillation waveform using the `scipy.optimize.curve_fit` function. The fitted waveform was then visualized, and the damped oscillation parameters, including amplitude, damping constant, angular frequency, and initial phase angle (Figure 3, lower left), were obtained and compared for each group. The mean \pm SD of the coefficient of determination (R^2) and the relative mean absolute error for each group were obtained as indices for evaluating the model.

Statistical Analysis

Continuous variables were expressed as mean \pm SD, and categorical data were expressed as counts and percentages. The normality of continuous variables was tested with the Shapiro-Wilk test, and the variability of continuous variables was tested with the Bartlett test. Once normality and equal variance were confirmed, 1-way analysis of variance was performed, and Tukey's HSD multiple comparison test was performed on variables for which the results were significant. Where normality and equal variance were not confirmed, a nonparametric Kruskal-Wallis test was conducted, with a Steel-Dwass multiple comparison test being applied to variables where the results were significant. Categorical variables were compared using Fisher exact test.

All statistical analyses were conducted in the Python environment, utilizing the `scipy.stats` module for 1-way analysis of variance and Kruskal-Wallis tests, the `statsmodels` package for post hoc tests, and the `rpy2` module for the Fisher exact test.

RESULTS

Patient Characteristics

Patients were predominantly male, with no significant difference in proportion between groups. There were significant differences in age, body dimensions (height, weight, and body mass index), hypertension, and arch type between groups (Table 1). The BAV group was older than the control group and the TBAD group. Weight and body mass index were higher in the TBAD group than in the control group. Hypertension was more common in the TBAD group than in the control and BAV groups. Arch type I was significantly more prevalent in the control group than in the TBAD group ($P = .0059$). No significant difference was found in the frequency of type III, although it was less common in the control group than in the TBAD and BAV groups.

Centerlines of the Thoracic Aorta after Data Standardization and Curve Regression Procedure

Figure 4 illustrates the centerline of the thoracic aorta following data scaling, coordinate transformation based on the optimal plane, and curve regression. The 180°

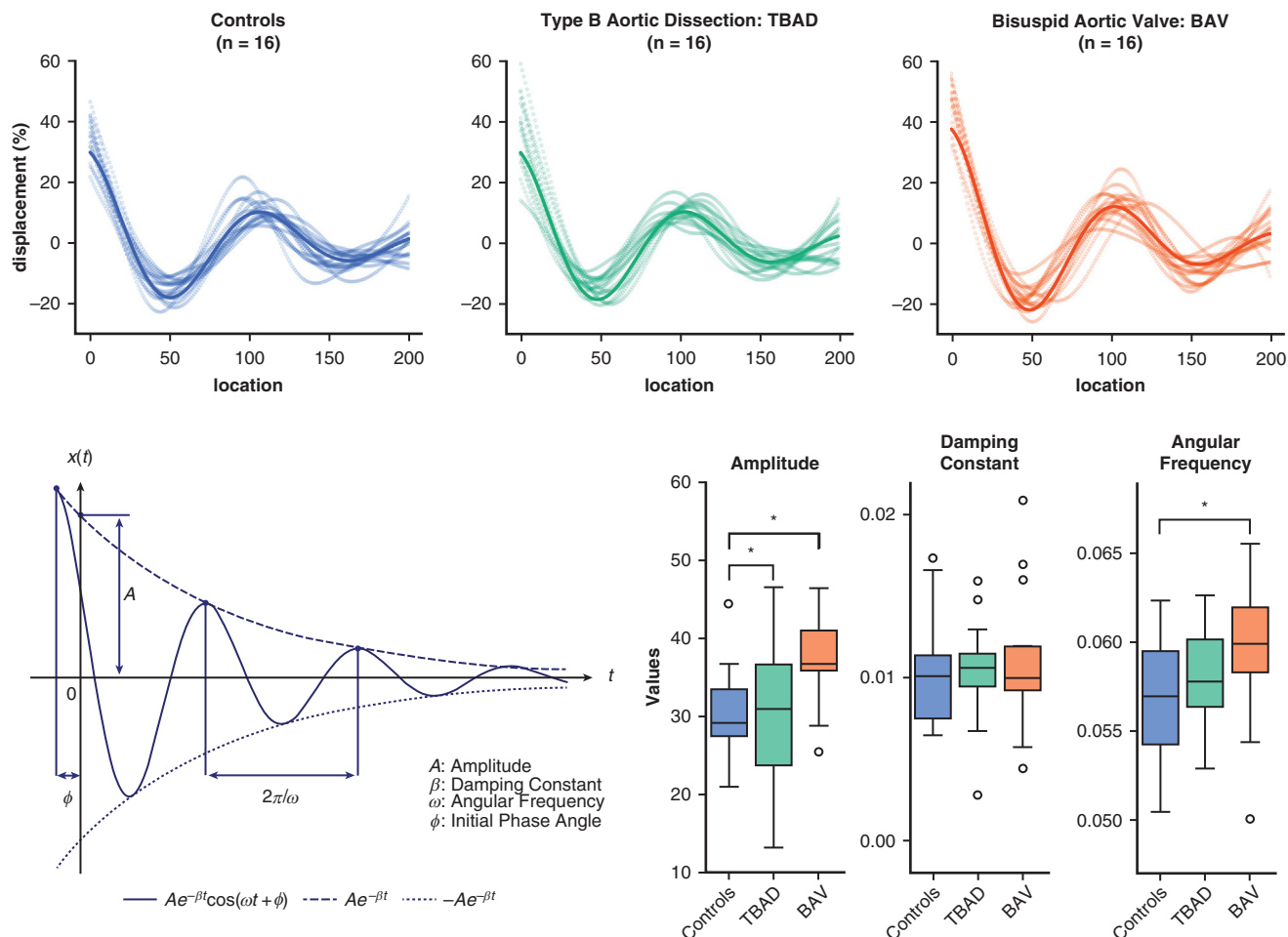


FIGURE 3. Damped oscillation model. Upper row displays actual measured transverse displacement data for all groups (controls, type B aortic dissection and bicuspid aortic valve) in the form of open circles and average curves after damped oscillation waveform fitting in **bold lines**. The damped oscillation model, including its parameters, is displayed in the lower left panel. The lower right panel displays a box plot of damped oscillation fitting parameters for all groups, including amplitude, damping constant, and angular frequency. The lower and upper borders of the box represent the lower and upper quartiles (25th and 75th percentiles), respectively. The middle horizontal line represents the median. The lower and upper whiskers represent the minimum and maximum values of non-outliers, respectively. Extra dots represent outliers. * $P < .05$.

horizontally rotated images of all cases and the average of each group are presented in [Video 1](#). The superimposition of all cases in the lower left panel shows considerable variation from AoR to AscAo and in DesAo. Comparing averages of the groups revealed differences from AoR to AscAo, in the distal arch, and in the obliteration of DesAo.

Intersection Points of Centerline and Optimal Plane

When the starting point of the centerline is set as A, the ending point as E, and intersection points of the centerline and the optimal plane as B, C, and D (in this order), the area between A and B is generally considered to correspond to AoR, between B and C to AscAo, between C and D to Arch, and between D and E to DesAo. Intersection points of the centerline and optimal plane serve as defining markers of anatomic location on the centerline ([Figure 1](#)). In the analysis of transverse displacement, which presents a damped

oscillation pattern ([Figure 2, lower left](#)), averages and SD of all cases of the first, second, and third sign transformation points were obtained. These values were: 24.0 ± 3.4 for B, 78.1 ± 6.9 for C, and 132.1 ± 8.2 for D. The average values were subsequently used as indicators of anatomical location in the analysis of curvature κ and torsion τ .

Curvature κ and Torsion τ

Curve regression with second and third derivatives as penalty terms was employed for smoothing purposes. However, the resulting curvature κ and torsion τ exhibited considerable variations and fluctuations, with torsion τ exhibiting the most pronounced fluctuations ([Figure E2](#)).

Curvature κ exhibited bimodal characteristics showing peaks in AscAo and Arch, with the latter being higher, in all groups ([Figure 5, upper middle and right](#)). Torsion τ , which was smoothed by the moving average, showed a

TABLE 1. Patient characteristics

	Control (n = 16)	Type B aortic dissection (n = 16)	Bicuspid aortic valve (n = 16)	P value
Age (y)	54.8 ± 9.6 (31-66)	53.7 ± 4.5 (47-62)	64.3 ± 14.9 (24-83)	.0061
Male sex	11/16 (68.8)	13/16 (81.3)	13/16 (81.3)	.56
Height (cm)	167.4 ± 7.1	168.5 ± 6.2	162.5 ± 7.9	.050
Weight (kg)	60.2 ± 11.5	70.6 ± 13.2	62.1 ± 9.6	.034
BMI	21.4 ± 3.0	24.7 ± 3.5	23.4 ± 2.4	.010
BSA	1.67 ± 0.18	1.80 ± 0.18	1.66 ± 0.16	.058
Hypertension	5/16 (31.3)	16/16 (100)	5/16 (31.3)	.000013
Arch type				
I	9/16 (56.3)	1/16 (6.3)	4/16 (25.0)	.0087
II	5/16 (31.3)	7/16 (43.8)	4/16 (25.0)	.6414
III	2/16 (12.5)	8/16 (50.0)	8/16 (50.0)	.053

Values are presented as mean ± SD (range) or n/N (%). BMI, Body mass index; BSA, body surface area.

positive value in AscAo and a negative change in the middle portion of Arch, in all groups (Figure 5, lower right).

New Evaluation Indices Based on Optimal Plane

Transverse displacement. Figure 6 (upper left panel) illustrates transverse displacements of each group, exhibiting a damped oscillation pattern. When comparing the mean of all displacements of individual cases between the 3 groups, a significant difference was detected ($P = .0083$). This difference was significant between the control and TBAD groups ($P = .015$) and between the control and BAV groups ($P = .035$).

Figure 6 (upper right panel) shows integral values for intervals classified by sign conversion points (T1, T2, T3, as illustrated in Figure 2). A comparison of the 3 groups revealed significant differences at T1 and T2 (T1: $P = .012$; T2: $P = .010$). The post hoc test indicated that the control and BAV groups differed significantly at T1 ($P = .016$) and that the TBAD and BAV groups differed significantly at T2 ($P = .0074$).

Anteroposterior displacement. Figure 6 (middle left panel) illustrates anteroposterior displacements of each group, exhibiting an inverted S-shaped pattern. When comparing the mean of all displacements of individual cases among the 3 groups, a significant difference was detected ($P = .010$). This difference was significant between the control and TBAD groups ($P = .0073$).

Figure 6 (middle right panel) shows integrated values of intervals classified by sign conversion points (AP1, AP2, as illustrated in Figure 2). A comparison of the 3 groups revealed significant differences at AP1 ($P = .0088$), and in the post hoc test, a significant difference was observed between the control and TBAD groups ($P = .0077$).

Longitudinal displacement. Figure 6 (lower left panel) illustrates longitudinal displacements for each group,

exhibiting an upward convex curve pattern. When comparing the mean of all displacements of individual cases among the 3 groups, a significant difference was detected ($P = 1.32 \times 10^{-6}$). This difference was significant between the control and TBAD groups ($P = .0014$) and between the TBAD and BAV groups ($P < .0001$).

Figure 6 (lower right panel) shows integrated values of intervals classified by sign transformation points (L1, L2, L3, as illustrated in Figure 2). A comparison of the 3 groups revealed significant differences in L1, L2, and L3 (L1, $P = 1.62 \times 10^{-6}$; L2, $P = .024$; L3, $P = .00015$). Post hoc tests yielded the following results. In L1, a significant difference was observed between the control and BAV groups ($P < .000001$) and between the TBAD and BAV groups ($P < .000001$). In L2, a significant difference was observed between the control and TBAD groups ($P = .024$). In L3, significant differences were observed between the control and TBAD groups ($P = .0018$) and between the TBAD and BAV groups ($P = .0003$).

Analysis of Damped Oscillation Patterns for Transverse Displacement

The fitting generally reflected the variation in measured data (Figure 3, upper row). Coefficients of determination (R^2) were 0.97 ± 0.12 for the control group, 0.95 ± 0.025 for the TBAD group, and 0.96 ± 0.018 for the BAV group. Relative mean absolute error were 0.16 ± 0.039 for the control group, 0.22 ± 0.055 for the TBAD group, and 0.19 ± 0.047 for the BAV group. A comparison of damping oscillation parameters among the three groups revealed significant differences in amplitude ($P = .0068$) and angular frequency ($P = .045$). The amplitude was significantly greater in the BAV group than in the control ($P = .013$) and TBAD groups ($P = .019$). Similarly, the angular

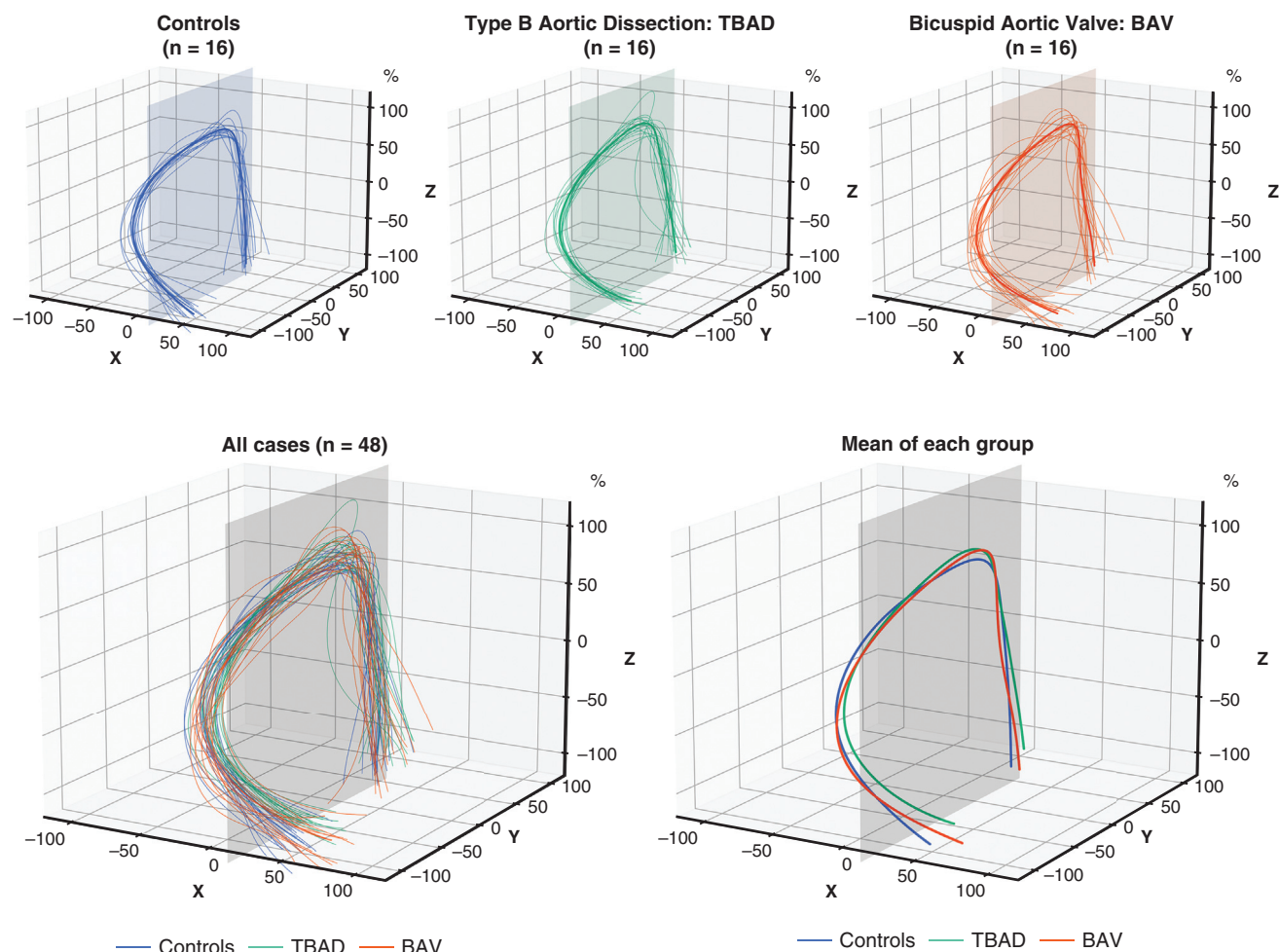


FIGURE 4. Centerline of thoracic aorta. Top row shows the centerline and its mean for each group. Bottom left panel shows all cases superimposed; bottom right panel shows the mean for each group.

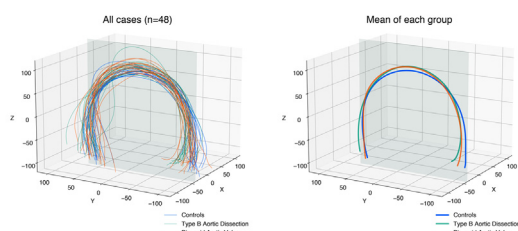
frequency was significantly higher in the BAV group than in the control group ($P = .035$) (Figure 3, lower right).

DISCUSSION

This study presents a novel analytical approach based on the optimal plane for the centerline analysis of the thoracic

aorta. This approach allowed for a quantitative assessment of disparities in the 3D morphology of the thoracic aorta among control, TBAD, and BAV groups.

In relation to TBAD and the 3D morphology of the thoracic aorta, previous studies have reported that the length of AscAo and Arch, as well as the respective angulation index, tortuosity index, and arch type III, are risk factors.^{4,13-15} In BAV, the length of AscAo to Arch, the tortuosity index, and its minimum angle have been reported to be associated with disease severity.¹⁶ The angulation index and tortuosity index in these reports are fundamentally distinct from curvature κ and torsion τ . Thoracic aortic length is a 1-dimensional measurement, and angulation index, tortuosity index, and arch type are indicators on a 2-dimensional plane and do not fully reflect the characteristics of the 3D curve. With regard to the relationship between BAV and the 3D morphology of the thoracic aorta, an intriguing study has been published indicating a correlation between the rotation of AoR and the severity of disease.¹⁷



VIDEO 1. The 180° horizontally rotated images of all cases and the average of each group. Video available at: [https://www.jtcvs.org/article/S2666-2736\(24\)00264-X/fulltext](https://www.jtcvs.org/article/S2666-2736(24)00264-X/fulltext).

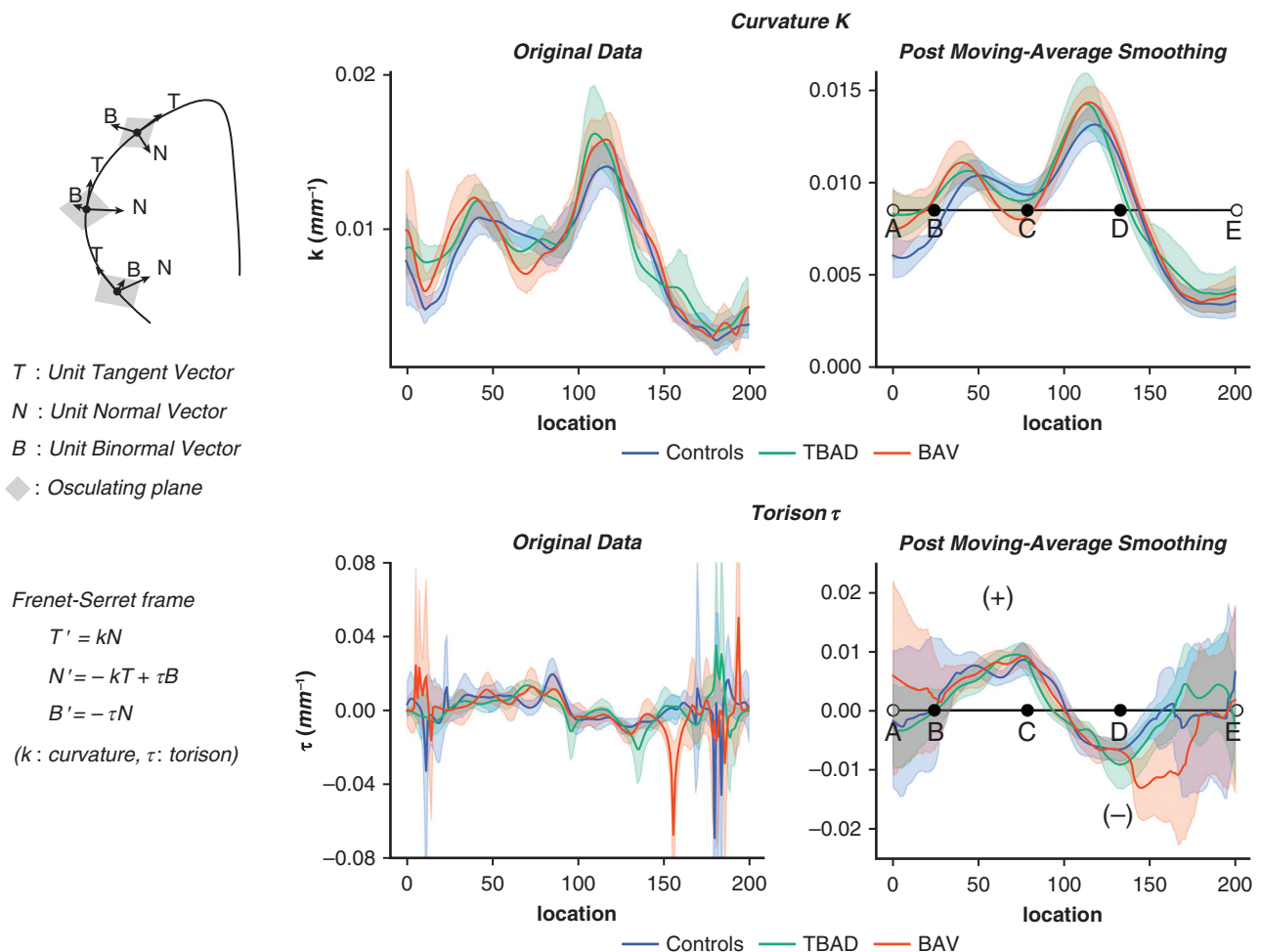


FIGURE 5. Curvature κ and torsion τ . *Left panel*, Diagram of the Frenet-Serret frame (TNB frame) and the osculating plane, as well as a relationship between curvature κ , torsion τ , and the TNB frame. *Upper middle and right panels* show curvature κ (*left half*; original data with 95% CI, *right half*; after moving-average smoothing). *Lower middle and right panels*, Torsion τ (*left half*; original data with 95% CI, *right half*; after moving-average smoothing). The area between A○ and B● is generally considered to correspond to the aortic root, between B● and C● to the ascending aorta, between C● and D● to the aortic arch, and between D● and E○ to the descending aorta. *T*, Unit tangent vector; *N*, unit normal vector; *B*, unit binormal vector. *TBAD*, Type B aortic dissection; *BAV*, bicuspid aortic valve.

Curvature κ and Torsion τ

This study presents 2 new findings regarding the 3D morphology of the thoracic aorta. First, curvature κ exhibited bimodal characteristics showing peaks in AscAo and Arch, with the latter being higher. Second, torsion τ underwent a transition from a positive value to a negative value within Arch, accompanied by a reversal in the direction of torsion from right-handed to left-handed. Further research is necessary to determine the anatomical significance of these findings and their relationship to disease.

Novel Analytical Approach Based on Optimal Plane

In the present study, the centerline of the thoracic aorta was divided into 3 representative features based on the

optimal plane. The analysis of these features allows for a systematic and comprehensive investigation of the morphology of the thoracic aorta, without the necessity for complex calculations such as curvature and torsion.

The mean of the centerline of each group provides a visual representation of the differences in 3D shape from AoR to AscAo, in the distal arch, and in the peripheral DesAo (Figure 4, lower right panel, and Video 1). The novel analytical approach based on the optimal plane enables quantification of differences from AoR to AscAo as differences in the interval integrals T1, T2, AP1, and L1 in each direction, differences in the distal arch as differences in the longitudinal interval integral L2, and differences in the peripheral DesAo as differences in the longitudinal interval integral L3 (Figures 2 and 6).

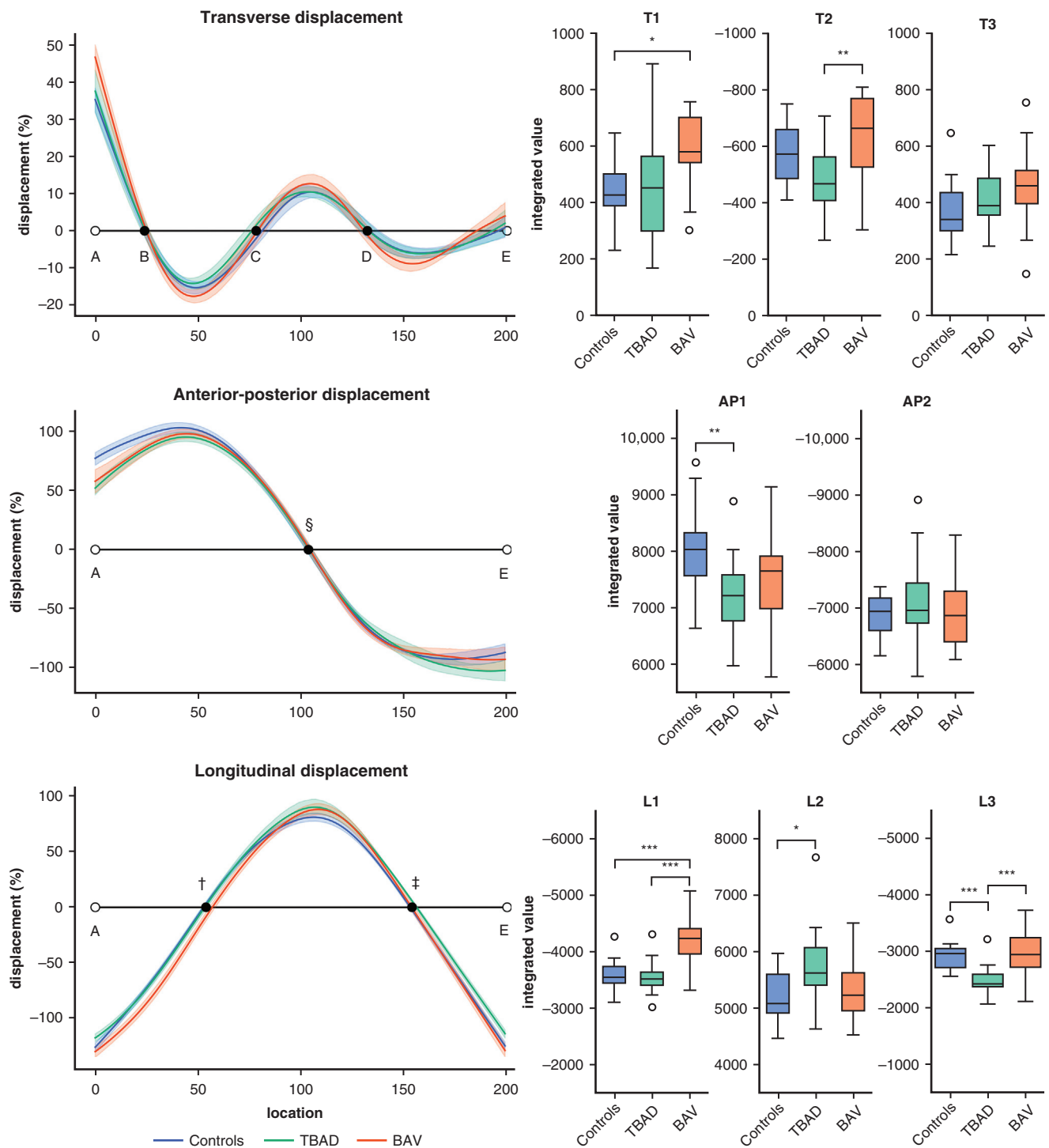


FIGURE 6. New evaluation indices based on optimal plane. Upper row displays transverse displacements for all groups, accompanied by 95% CI and integral values for intervals classified by sign conversion points (T1, T2, T3) as box plots. The middle row presents anteroposterior displacements for all groups, accompanied by 95% CIs and integral values for intervals classified by sign conversion points (AP1, AP2) as box plots. The lower row displays longitudinal displacements for all groups, accompanied by 95% CI and integral values for intervals classified by sign conversion points (L1, L2, L3) as box plots. The lower and upper borders of the box represent the lower and upper quartiles (25th and 75th percentiles), respectively. The middle horizontal line represents the median. The lower and upper whiskers represent the minimum and maximum values of nonoutliers, respectively. Extra dots represent outliers. * $P < .05$. ** $P < .01$. *** $P < .005$.

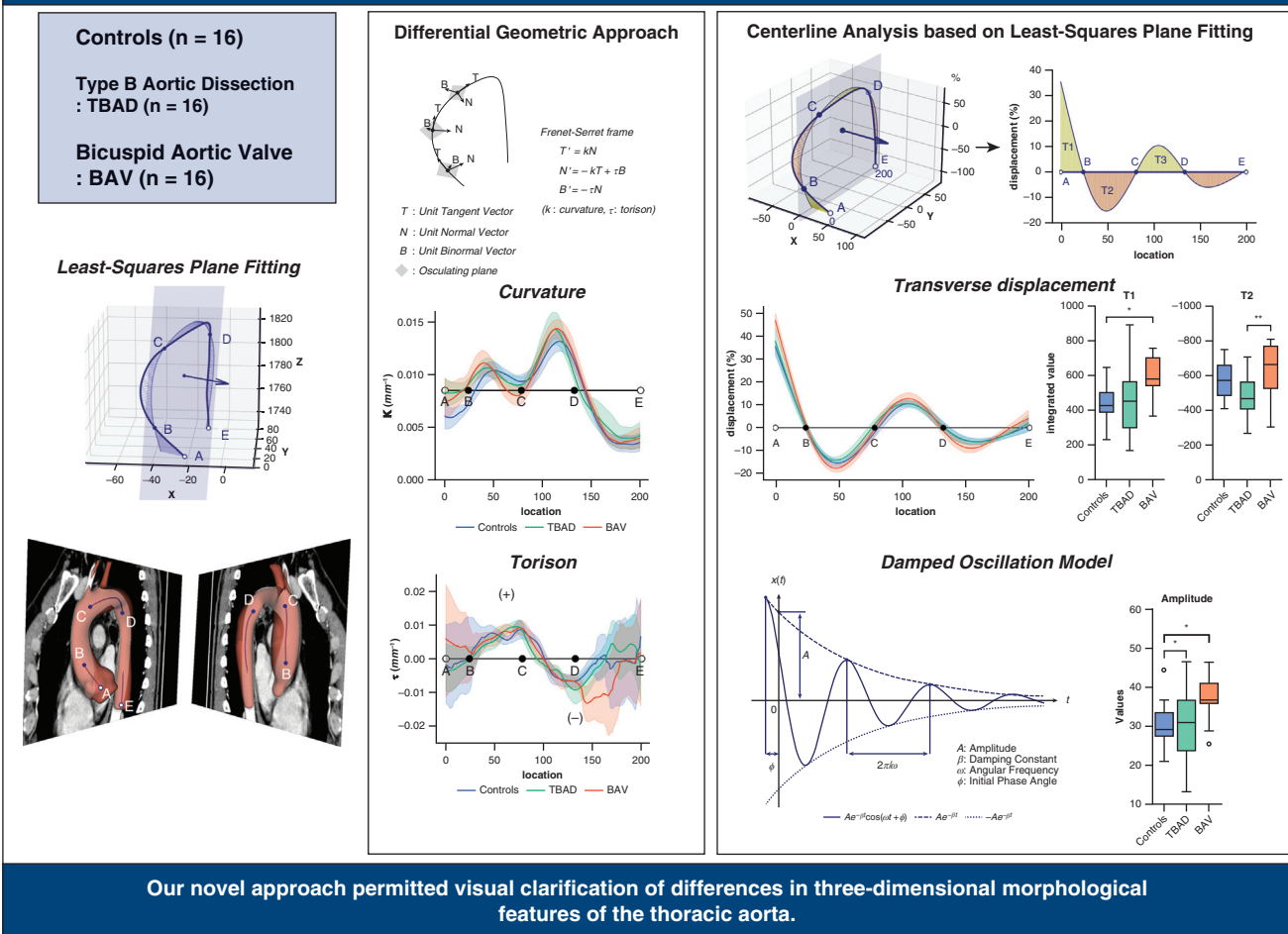
Three-Dimensional Morphometry of the Human Thoracic Aorta using Centerline Analysis based on Least-Squares Plane Fitting


FIGURE 7. Graphical abstract. TBAD, Type B aortic dissection; BAV, bicuspid aortic valve.

Damped Oscillation Pattern for Transverse Displacement

The present study revealed significant differences in amplitude and angular frequency among the damped oscillation parameters. In particular, amplitude was found to be significantly larger in the TBAD and BAV groups compared with the controls group. As the amplitude of the damped oscillation pattern increases, it is reasonable to anticipate an elevated risk of dissection and aneurysm formation, influenced by its effect on the blood flow pattern in the thoracic aorta. These parameters appear to be potentially important in linking morphology and disease.

Study Limitations

- This is a preliminary study with a limited number of cases. At this time, we are unable to discuss the anatomical significance of differences in the shape of each group as indicated by the new evaluation index, or their relationship to disease. However, we hope that our approach will provide a basic framework for properly understanding the 3D morphology of the thoracic aorta, which is characterized by bending and twisting.
- With regard to patient background, it was not possible to assume the same age range for each group. In particular, the BAV group was significantly older, which may be

attributed to additional age-related shape changes in the BAV group.

- It is evident that motion artifacts exert a considerable influence on the centerline analysis of AoR in proximity to the heart. Therefore, it is important to perform CT imaging with ECG synchronization to eliminate the influence of motion artifacts.
- With regard to adaptation of the damped oscillation model to transverse displacements, the evaluation should be repeated with a greater number of cases to ascertain whether or not the model is optimal.

CONCLUSIONS

As a novel approach to characterize the 3D morphology of the thoracic aorta, we developed a centerline analysis based on least-squares plane fitting. The intersection of the optimal plane (least-squares plane) and the centerline was found to generally coincide with the transition zone of Root, AscAo, Arch, and DesAo. Furthermore, the distance between the optimal plane and the centerline exhibited a damped oscillation pattern. Our novel approach permitted visual clarification of differences in 3D morphological features of the thoracic aorta (Figure 7). In the future, this approach may be utilized as a diagnostic indicator to distinguish severe cases and high-risk cases.

Conflict of Interest Statement

The authors reported no conflicts of interest.

The *Journal* policy requires editors and reviewers to disclose conflicts of interest and to decline handling or reviewing manuscripts for which they may have a conflict of interest. The editors and reviewers of this article reported no conflicts of interest.

The authors thank the staff at Seirei Mikatahara General Hospital for their invaluable support in conducting clinical research.

References

1. Isselbacher EM, Preventza O, Hamilton Black J III, et al. 2022 ACC/AHA guideline for the Diagnosis and Management of Aortic Disease: a report of the American Heart Association/American College of Cardiology Joint Committee on Clinical Practice Guidelines. *Circulation*. 2022;146(24):e334-e482.
2. Mori D, Yamaguchi T. Numerical fluid dynamics of the blood flow in the thoracic aorta with respect to the pathogenesis of the aortic aneurysm. *Research Rep*. 2009; 44:29-34. https://doi.org/10.24704/hnctech.44.0_29
3. Della Corte A, Rubino AS, Montella AP, et al. Implications of abnormal ascending aorta geometry for risk prediction of acute type A aortic dissection. *Eur J Cardiothorac Surg*. 2021;60(4):978-986.
4. Cao L, Lu W, Ge Y, et al. Altered aortic arch geometry in patients with type B aortic dissection. *Eur J Cardiothorac Surg*. 2020;58(4):714-721.
5. Bissell MM, Hess AT, Biasioli L, et al. Aortic dilation in bicuspid aortic valve disease: flow pattern is a major contributor and differs with valve fusion type. *Circ Cardiovasc Imaging*. 2013;6(4):499-507.
6. Hohri Y, Numata S, Itatani K, et al. Prediction for future occurrence of type A aortic dissection using computational fluid dynamics. *Eur J Cardiothorac Surg*. 2021;60(2):384-391.
7. Salmasi MY, Pirola S, Mahuttanatan S, et al. Geometry and flow in ascending aortic aneurysms are influenced by left ventricular outflow tract orientation: detecting increased wall shear stress on the outer curve of proximal aortic aneurysms. *J Thorac Cardiovasc Surg*. 2023;166(1):11-21.
8. Kobayashi M, Hoshina K, Nemoto Y, et al. A penalized spline fitting method to optimize geometric parameters of arterial centerlines extracted from medical images. *Comput Med Imaging Graph*. 2020;84:101746.
9. Brummer AB, Hunt D, Savage V. Improving blood vessel tortuosity measurements via highly sampled numerical integration of the Frenet-Serret equations. *IEEE Trans Med Imaging*. 2021;40(1):297-309.
10. Gallo D, Vardoulis O, Monney P, et al. Cardiovascular morphometry with high-resolution 3D magnetic resonance: first application to left ventricle diastolic dysfunction. *Med Eng Phys*. 2017;47:64-71.
11. Fukui T, Asama H, Kimura M, Itoi T, Morinishi K. Influence of geometric changes in the thoracic aorta due to arterial switch operations on the wall shear stress distribution. *Open Biomed Eng J*. 2017;11:9-16.
12. Zhang X, Luo M, Fang K, et al. Application of 3D curvature and torsion in evaluating aorta tortuosity. *Commun Nonlinear Sci Numer Simul*. 2021;95:105619.
13. Marrocco-Trischitta MM, Rylski B, Schofer F, et al. Prevalence of type III arch configuration in patients with type B aortic dissection. *Eur J Cardiothorac Surg*. 2019;56(6):1075-1080.
14. Lescan M, Veseli K, Oikonomou A, et al. Aortic elongation and Stanford B dissection: The Tübingen aortic pathoanatomy (TAIPAN) project. *Eur J Vasc Endovasc Surg*. 2017;54(2):164-169.
15. Sun L, Li J, Liu Z, et al. Aortic arch type, a novel morphological indicator and the risk for acute type B aortic dissection. *Interact Cardiovasc Thorac Surg*. 2022; 34(3):446-452.
16. Fujiwara J, Oritani M, Takagi H, et al. Aortic elongation in bicuspid aortic valve with aortic stenosis assessed by thin-slice electrocardiogram-gated computed tomography. *Int Heart J*. 2022;63(2):319-326.
17. Mori S, Yamashita T, Takaya T, et al. Association between the rotation and three-dimensional tortuosity of the proximal ascending aorta. *Clin Anat*. 2014;27(8): 1200-1211.

Key Words: thoracic aorta, 3-dimensional morphology, centerline analysis, least-squares plane fitting, curvature κ , torsion τ , damped oscillation

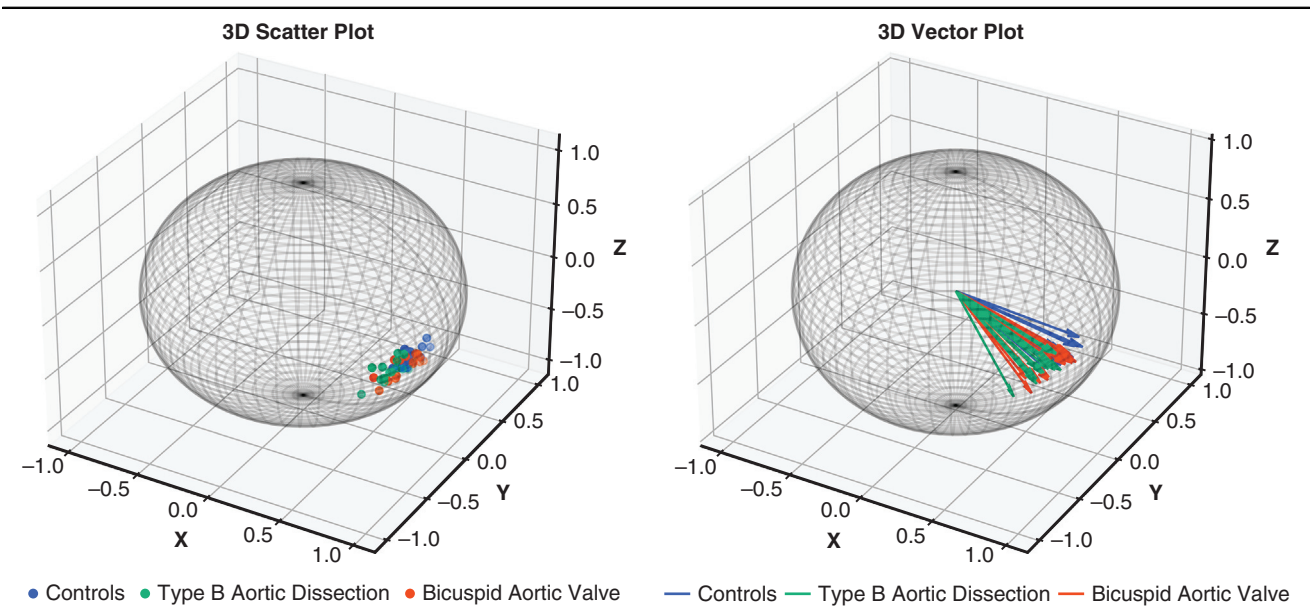


FIGURE E1. The normal vector of the least-squares plane. The left panel shows that the components of the unit normal vectors are plotted on the sphere for each group. The right panel shows the unit normal vectors for each group. 3D, Three dimensional.

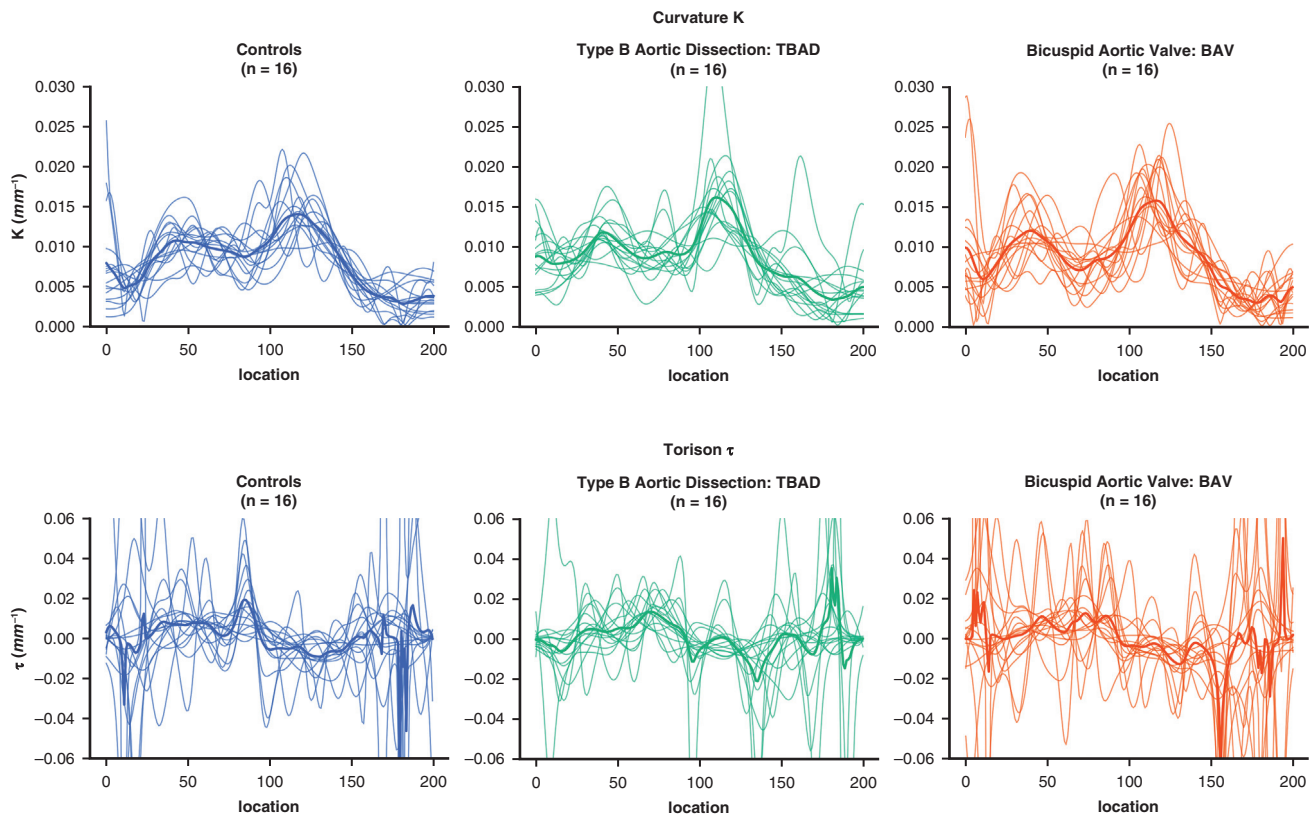


FIGURE E2. Curvature κ and torsion τ . The upper row shows curvature κ and its mean for each group. The lower row shows torsion τ and its mean for each group.